DESIGN AND EXPERIMENTAL STUDY OF A SINGLE LONGITUDINAL AXIAL FLOW THRESHING AND SEPARATION DEVICE WITH COMBINED RASP-BAR AND NAIL-TOOTH THRESHING ELEMENTS FOR MILLET

。 谷子纹杆-钉齿组合式单纵轴流脱粒分离装置设计与试验研究

Jun-hui ZHANG¹⁾, Shu-juan YI^{*1)}, Dong-ming ZHANG¹⁾, Tian-min YI²⁾

¹⁾College of Engineering, Heilongjiang Bayi Agricultural University, Daqing/P.R.China
²⁾Beijing Polytechnic, Beijing, 100176, China
Tel: +86-459-13836961877; E-mail: yishujuan_2005@126.com
Corresponding author: Shu-juan YI
DOI: https://doi.org/10.35633/inmateh-77-65

Keywords: millet, combined threshing element, threshing and separation device, experimental investigation

ABSTRACT

In response to the problems of high glume cluster rate, significant losses, and limited adaptability during millet combine harvesting in China, an independent test bench for a single longitudinal axial-flow threshing and separation device was designed and constructed. Millet moisture content, feeding rate, and threshing drum rotational speed were selected as the influencing factors, while impurity rate, glume cluster rate, and total loss rate were used as evaluation indices. Single-factor experiments and orthogonal rotational combination tests were conducted. The experimental results show that the order of influence on impurity rate, glume cluster rate, and total loss rate is: moisture content > rotational speed > feeding rate. The optimal operating parameters obtained were: moisture content of 24.82%, feeding rate of 2.25 kg/s, and drum rotational speed of 835 r/min. Under these conditions, the impurity rate reached 31.90%, the glume cluster rate was 21.56%, and the total loss rate was 0.72%. These findings provide a technical reference for the future design and development of single longitudinal axial flow threshing and separation devices specialized for millet harvesting.

摘要

针对我国谷子联合收获过程中存在碎谷码率高、损失大、适应性差等问题,自行设计搭建了组合式单纵轴流脱分分离装置试验台,选取谷子含水率、喂入量、滚筒转速为影响因素,以碎谷码率、含杂率、总损失率为指标,分别进行了单因素试验和正交旋转组合试验。试验结果表明:对含杂率、碎谷码率和总损失率的作用顺序为含水率>转速>喂入量。获得最优试验参数为:含水率24.82%,喂入量2.25kg/s,转速835r/min。在此条件下,含杂率为31.90%,碎谷码率为21.56%,总损失率为0.72%。试验结果为今后适用于谷子的单纵轴流脱粒分离装置的设计和研究提供参考。

INTRODUCTION

With the continuous improvement of living standards in China and the growing emphasis on dietary diversification, minor grain crops such as millet are receiving increasing public recognition. In comparison to major crops such as rice, wheat, corn, and soybeans, the level of mechanization in millet production—particularly during the harvesting stage—remains relatively low. To investigate the influence of the unique growth and material characteristics of grain on the performance of harvesting machinery, Gorji A evaluated the grain's resistance to fracture by employing fracture force and fracture energy as key indicators, and concluded that moisture content and loading rate exert a significant effect on these mechanical properties (Gorji A. et al., 2010). Through single-factor experiments and response surface methodology, the mechanical properties of mature millet straw were investigated, the order of significance of experimental factors was determined, and the optimal combination of parameters was identified (Yanqing et al., 2018; Zhang et al., 2019). To investigate the influence of various parameters on the performance of grain threshing devices, scholars both domestically and internationally have conducted extensive experimental studies on crops such as rice, wheat, corn, and soybeans, and have analyzed the interrelationships among mechanical efficiency, threshing efficiency, and seed breakage rate (Maundc et al., 2011; Atis et al., 2012; NNAM et al., 2025; Martynas et al., 2025).

Jun-hui Zhang, Ph.D.; Shu-juan Yi, Prof. Ph.D.; Dong-ming Zhang, Ph.D.; Tian-min YI, master degree

The influence of machine and crop parameters on mechanical grain damage during rice threshing was investigated (Solomon et al., 2024). The impact of the rectangular sharp-tooth threshing cylinder structure on wheat threshing performance was assessed (Tiwari et al., 2018). A double longitudinal-axis flow corn threshing device with a high feeding capacity was designed and experimentally investigated, offering a reference for the development and design of similar high-capacity threshing equipment (Mingrui et al., 2025). The threshing process and associated grain damage in corn were systematically examined (Fozilov G. et al., 2025; Dainius et al., 2023). To address the issue of soybean shattering during the harvesting process, experiments were carried out to determine the optimal combination of parameters, resulting in a reduced soybean shattering rate (Hou et al., 2012; Panpan et al., 2025). Furthermore, the threshing device for soybeans was enhanced to improve efficiency and reduce losses (Wuttiphol et al., 2018; Ukatu et al., 2006). Amir Hossein Mirzabe et al. developed a non-destructive jet-impact threshing device for sunflower harvesting and experimentally determined the optimal parameter values, including nozzle diameter, distance between the nozzle and flower disc, impact angle, and air pressure (Amir et al., 2015; Amir et al., 2016). Based on the characteristics of millet, a semi-feed threshing device test bench and a double-roller transverse axial flow combine harvester were designed, and experimental research was carried out. Through this research, a regression model was established, and the optimal combination of device parameters was obtained (Luo et al., 2016; Wang et al., 2016; Kang et al., 2017). To address the challenges of poor adaptability and high glume cluster during the combined harvesting of millet, this study investigates the influence of various experimental factors on the threshing and separating performance of millet harvesting machinery. Using Longgu 31 as the experimental material, a single longitudinal axial flow threshing and separating test bench with the rasp-bar and nail-tooth combined threshing element was independently designed and constructed. Single-factor and orthogonal rotational experiments on millet threshing and separation were conducted, providing a scientific basis for the design and development of single longitudinal axial flow threshing and separating devices tailored to the characteristics of millet.

MATERIALS AND METHODS

1. Structure and working principles of the single longitudinal axial flow threshing and separation device

The single longitudinal axial flow threshing and separation device utilizing the rasp-bar and nail-tooth combined threshing element is shown in Fig. 1. This device primarily comprises the feeding mechanism, threshing cylinder, cover plate, combined threshing elements, concave plate, material collection trolley, and control system.



Fig. 1 - Single longitudinal axial flow threshing and separation device

1. Conveyor; 2. Feeding mechanism; 3. Threshing cylinder; 4. Material collection trolley; 5. Control system

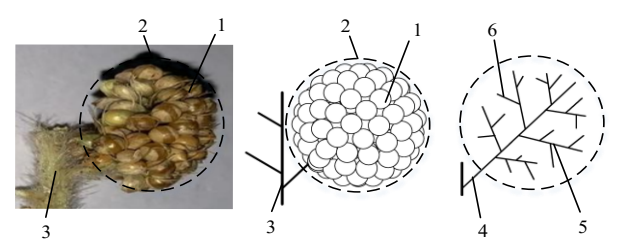


Fig. 2 - Schematic diagram of millet ear branching

1.Grain of millet; 2. Glume cluster; 3. Cob; 4. Primary branch; 5. Secondary branch; 6. Tertiary branch

The selection of appropriate threshing components is based on the growth characteristics of the crop and its material property parameters. The millet ear consists of the cob, glume clusters, and grains. Positioned at the apex of the millet plant, the ear typically exhibits a spindle or cylindrical shape, with an average length ranging from 20 to 25 cm (as illustrated in Fig. 2). The branching structure of the ear is organized into three levels. Primary branches are systematically arranged around the cob, while secondary and tertiary branches exhibit a more random distribution on the primary branches, contributing to the variability in glume cluster shapes. Each glume cluster comprises multiple branches, spikelet flowers, and awns, and generally appears spherical with diameters between 8 and 15 mm. The number of glume clusters ranges from 80 to 120, and each cluster bears between 50 and 110 grains. A schematic diagram illustrating the branching structure of the millet ear is presented in Fig. 2. Given the aforementioned characteristics of millet ears, the threshing process is primarily achieved through rubbing action. Accordingly, a combined threshing component of the rasp-bar

and nail-tooth is employed (as illustrated in Fig. 3). The front section of the threshing cylinder incorporates a grooved-cylinder structure that utilizes rubbing interactions among the grooved cylinder, crop material, and concave plate to detach grains from the ear. The rear section is equipped with spikes, which, through their stirring action, loosen the material inside the threshing chamber and enhance the probability of grain separation through the straw layer and concave openings.

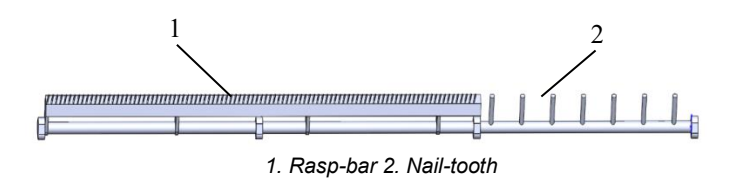


Fig. 3 - Rasp-bar and nail-tooth combined threshing and separation element

Fig. 4 - Concave plate

60

Table 1 Structural parameters of rasp-bar and nail-tooth combined threshing

Table 2

and separation element **Parameters** Value Length of the rasp-bar section/(mm) 900 Length of the combined threshing element/(mm) 1400 Number of the nail-tooth 7 Nail tooth height/(mm) 70 Nail tooth diameter /(mm) 10 Nail tooth spacing/(mm)

Main parameters of Single longitudinal flow threshing and separation test bed

Parameters Value Feeding speed of transport device (m/s) 0-5 Length of axial flow threshing cylinder (mm) 1895 Diameter of axial flow threshing cylinder (mm) 632 Rotational speed of axial-flow threshing cylinder (r/min) 0-1200 Threshing gap (mm) 7 Threshing element rasp-bar and nail-tooth Grid Structural form of concave plate Wrap angle of concave plate (°) 180 Gap between concave plate ribs (mm) 11

The length of the concave plate is typically determined based on the length of the threshing cylinder, with a wrap angle of 180° selected for optimal performance. The primary types of concave plate configurations are grid-type and perforated-type. The grid-type concave plate offers advantages such as high structural strength, excellent rigidity, larger sieve openings, and superior threshing and separation efficiency. In contrast, the perforated-type concave plate features a simpler design, ease of manufacturing, and reduced friction between the crop material and the concave surface, which helps minimize larger impurities in the threshed output. Given the objective of this study—to address the issues of poor threshing performance and high grain loss during millet harvesting—the grid-type concave plate was selected (as illustrated in Fig. 4). The selected grid diameter is 4.30 mm, with a transverse grid width of 10.80 mm.

A control system is integrated into the setup to enable real-time adjustment of the threshing cylinder speed, with an adjustable range of 0-1200 rpm. The receiving unit consists of multiple collection buckets, the dimensions of which are designed to accommodate the experimental requirements. During testing, the receiving unit is used to collect threshed material from different positions of the threshing and separation device. Additional key structural and operational parameters of the longitudinal axial flow threshing and separation test bench are summarized in Table 2.

2. Test program design

(1) Experimental Conditions

At the Harvesting Laboratory of Heilongjiang Bayi Agricultural University, threshing and separation experiments on millet were conducted using the single longitudinal axial flow threshing and separation device test bench. The experimental material consisted of Longgu 31 millet cultivated in Daqing City, Heilongjiang Province. The millet was manually harvested and collected in the laboratory.

A 15-meter-long conveyor belt was employed to simulate the forward motion of a combine harvester and continuously feed the millet into the threshing component to carry out the threshing test.

The tests were conducted under the following conditions: a concave bar diameter of 4.30 mm, concave cross-bar width of 10.80 mm, a total of 92 concave bars and 38 concave cross-bars, six rasp-bar and nail-tooth combined threshing elements, a millet straw-to-grain ratio of 1.61, and a grain density of 1053 kg/m³. Each test was repeated three times, and the average value was used for analysis.

(2) Test Method

Since the moisture content, feeding rate, and rotational speed significantly influence the threshing and separating performance of the combined single longitudinal axial flow threshing and separation device, these three parameters were selected as experimental factors. The glume cluster rate, impurity rate, and loss rate were chosen as the experimental indicators. Considering the limitations of indoor experimental conditions, the feeding rate was set within the range of 1.5 kg/s to 3 kg/s. The moisture content of mature grain was measured using an automatic moisture measurement instrument (as shown in Fig. 5), resulting in a determined moisture content range of 17% to 32%. The rotational speed exhibited a relatively wide adjustable range. Therefore, discrete element software EDEM was employed to simulate the threshing and separating performance at various rotational speeds to determine an appropriate experimental range. After defining the ranges of all experimental factors, single-factor experiments were conducted to clarify the interaction effects among grain moisture content, drum rotational speed, and feeding rate on the threshing and separating performance. Based on the results of these single-factor experiments, factor level coding was performed. A three-factor five-level orthogonal rotational combination experimental scheme was then designed using standard tables (as shown in Table 3), and multi-factor experiments were carried out. Regression analysis was conducted on the experimental results to derive regression equations for each experimental indicator in relation to the experimental factors, and interaction curves illustrating the effects of the experimental factors on the indicators were obtained.



Fig. 5 - Automatic moisture measuring instrument

(3) EDEM Simulation Experiment

(1) Simulation modeling

The millet ear structure was modeled based on its branching structure. The simulation model adopted the millet grain as the fundamental unit. Grain clusters were formed by aggregating a specific number of grain particles, while the entire millet ear was constructed through bonding keys that connected these clusters. Based on the morphological analysis of the millet ear's components and considering the need to balance modeling accuracy with computational efficiency, the final modeling scheme was as follows: the overall contour of the millet ear was represented by a cylinder with a circular cross-section diameter of 22 mm and a height of 210 mm. Both the grain clusters and individual grains were modeled as spheres, where the radius of the grain cluster sphere was 4 mm and the radius of the individual grain sphere was 0.75 mm. Each millet ear contained

100 grain clusters, with the number of grains in each cluster determined by the volume relationship of the spheres using formula (1).

$$\begin{cases} \alpha \cdot V_{Real} = N \cdot V_{Fraction} \\ V_{Real} = \frac{4}{3}\pi R^3, V_{Fraction} = \frac{4}{3}\pi r^3 \end{cases}$$
 (1)

where N is the number of grains to fill, α is the filling coefficient, which is 0.56 for spherical particles, V_{Real} is the volume of glume cluster, $V_{Fraction}$ is the volume of the grain sphere, R is the radius of glume cluster, r is the radius of the grain sphere.

Based on the aforementioned formula, N is approximately 84. To minimize the internal contact stress among grains post-filling, the number of grains N in this model is rounded down to 80.

The modeling process can be primarily divided into three stages: glume cluster filling, ear filling, and grain generation.

Glume Cluster Filling: A three-dimensional spherical model representing the contour of the glume cluster was constructed and imported into the Geometry module of EDEM to serve as the particle container. To improve system stability and computational efficiency, the contact coefficient was set to 0.01 during filling. A particle factory was then defined within the spherical region to generate grain particles. After all particles were naturally deposited and reached a stable state (Fig. 6(a)), the three-dimensional coordinate data of the grains were extracted and stored.

Grain Ear Filling: Using a similar procedure, the millet ear contour model was imported, and spherical glume-cluster particles together with grain particles were generated. The bonding contact model was selected for particle interactions, and a particle factory was created within a cylindrical region to generate the particles. After the system reached a stable state, the API-generated particles were replaced with the actual particles, and the glume-cluster particles were substituted with grain particles based on the grain coordinates obtained from the glume cluster filling stage. This process resulted in the formation of bonding bonds, as shown in Fig. 6(b).

Grain Generation: First, a compressed grain space was constructed using a press plate to eliminate voids between grains as much as possible. The three-dimensional coordinates of all grain particles were then extracted and saved. Next, the grain particles were generated using the quick-filling API, ensuring that all grains were created instantly at the beginning of the simulation according to the saved coordinates. Simultaneously, bonding bonds were established to connect the grains, as illustrated in Fig. 6(c).

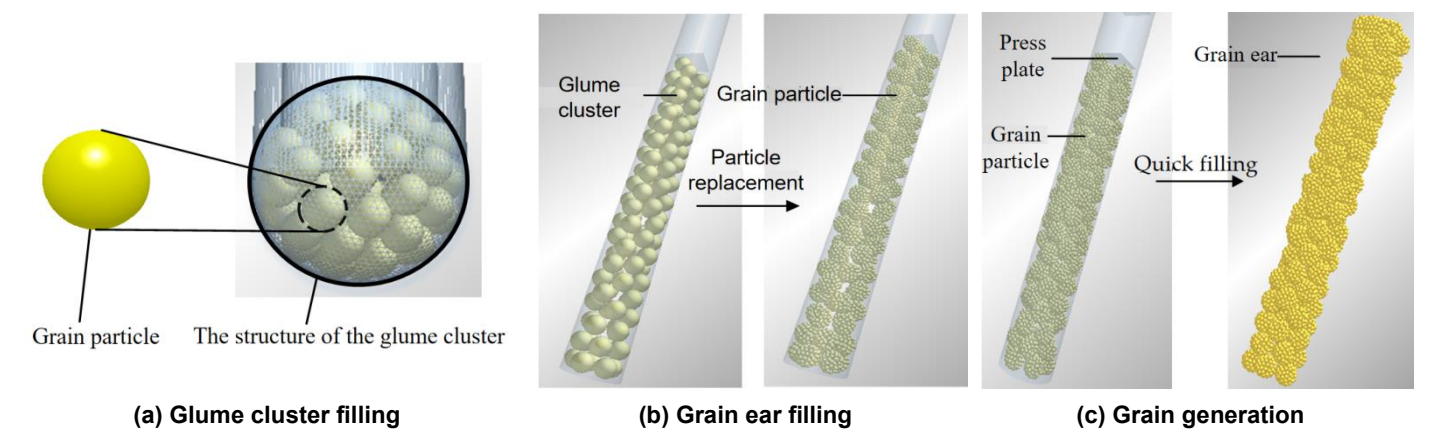
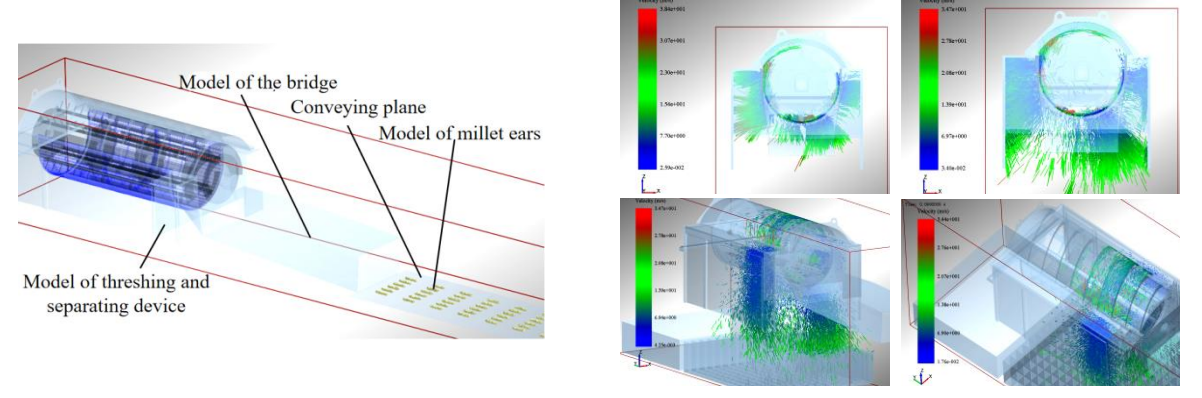


Fig. 6 - Schematic diagram of each stage of modeling

(2)Simulation Procedure

The discrete element simulation conducted in EDEM consisted of three primary stages: preprocessing, simulation execution, and post-processing. The detailed procedure for simulating the millet dehusking process is as follows. First, the model of the threshing and separation device was imported into EDEM. A receiving system composed of 14×14 cubic collection bins, each measuring 100×100×300 mm, was then constructed beneath the device to quantify particle distribution. Spherical millet particles with a radius of 0.75 mm were generated, and the bonding contact model was selected according to the particle interaction characteristics. The rotational motion of the threshing drum and the linear motion of the conveying plane were subsequently

defined. For each simulation run, a total of 50 millet ears were introduced. The overall simulation workflow is shown in Fig. 7.



(a) Development of millet ears

(b) Simulation of threshing and separation

Fig. 7 - Simulation process

RESULTS

1. EDEM simulation results

EDEM was employed to simulate the threshing and separating process of millet within a single longitudinal axial flow threshing and separation device with the rasp-bar and nail-tooth combined threshing element, under varying rotational speeds. The cumulative separation rate at each axial coordinate position was calculated and analyzed. The simulation results are presented in Fig. 8.

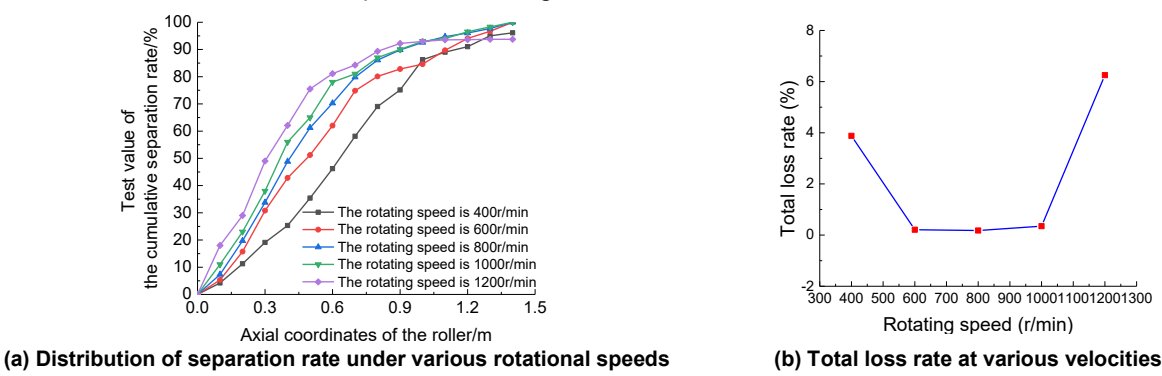


Fig. 8 - EDEM simulation results

As shown in Fig. 8(a), the cumulative separation rate of grains in the rasp-bar section increases with increasing rotational speed. Once the grains enter the nail-tooth section, the rate of increase in cumulative separation gradually diminishes. As illustrated in Fig. 8(b), at rotational speeds of 600 r/min, 800 r/min, and 1000 r/min, the total loss rate approaches 0%. In contrast, at 400 r/min and 1200 r/min, the loss rates are 3.88% and 6.25%, respectively.

When the rotational speed is too low, the threshing components exert insufficient rubbing and impact forces on the crop, resulting in incomplete separation of some grains from the panicle. Conversely, when the rotational speed is excessively high, the residence time of millet in the threshing and separation device becomes too short, reducing the effectiveness of interactions between the crop and the threshing elements. This also leads to incomplete grain separation. Based on the simulation results, the effective rotational speed range for the tests is 600-1000 r/min.

2. Analysis of the Results of Single-Factor Experimental

(1) A single-factor experiment on the moisture content of millet was carried out under a feeding rate of 2 kg/s and a rotational speed of 800 r/min. The selected moisture content levels of millet were 17%, 21%, 25%, 29%, and 33%, respectively. As shown in Fig. 9(a), with an increase in grain moisture content, the impurity rate initially decreases and subsequently increases, while the overall trend of the glume cluster rate curve exhibits an upward trajectory. The lowest impurity rate of 18.29% is observed at a moisture content of 29%. The minimum glume cluster rate of 19.87% occurs at a moisture content of 33%. With increasing grain moisture

content, the total loss rate all demonstrate a trend of first increasing and then decreasing. The lowest total loss rate of 0.12% is recorded at a moisture content of 17%.

- (2) A single-factor experiment on feeding rate was conducted under a rotational speed of 800 r/min and a moisture content of 25%. As shown in Fig. 9(b), when the feeding rate increases from 1 kg/s to 3 kg/s, the impurity rate curve initially decreases and subsequently increases, whereas the glume cluster rate curve first rises and then declines. The impurity rate reaches its minimal value of 24.50% at a feeding rate of 1.5 kg/s, and the glume cluster rate attains its peak of 14.75% at a feeding rate of 1.0 kg/s. With increasing feeding rate, the total loss rate first decrease and then increase. The total loss rate reaches its minimum value of 0.33% at a feeding rate of 2.0 kg/s.
- (3) A single-factor test on rotational speed was conducted under a feeding rate of 2 kg/s and a moisture content of 25%. As shown in Fig. 9(c), when the speed increases from 600 r/min to 1000 r/min, the impurity rate curve exhibits an overall upward trend, whereas the glume cluster rate curve demonstrates a downward trend. The glume cluster rate curve becomes relatively stable when the speed exceeds 900 r/min. At the maximum speed of 1000 r/min, the impurity rate reaches a peak value of 34.37%, while the glume cluster rate attains its minimum value of 19.11%. When the speed is below 800 r/min, the variations in both the impurity rate and the glume cluster rate are relatively mild. However, when the speed exceeds 800 r/min, the rate of change for both indicators increases significantly. With increasing rotational speed, the total loss rate initially rise and subsequently decline. At a speed of 1000 r/min, the total loss rate reaches its minimum value of 0.34%.

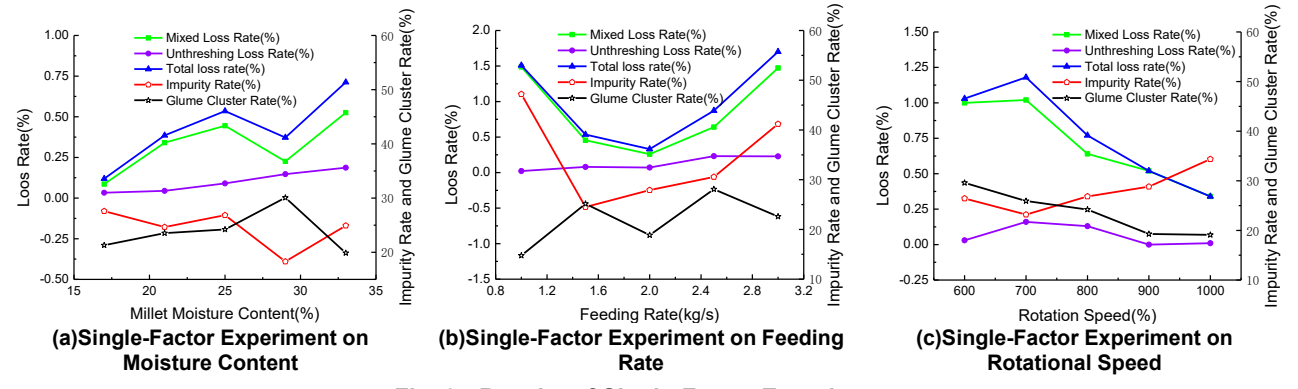


Fig. 9 - Results of Single-Factor Experiment

In conclusion, the moisture content of 25% for millet, feeding rate of 2 kg/s, and rotational speed of 800 r/min are taken as the 0-level factors in the multi-factor experiment.

3. Analysis of the Results of Multi-Factor Experiments

(1) Regression analysis of experimental results

Orthogonal rotation combination design scheme and results

Table 4

Experime nt Number	Moisture Content X ₁ (%)	Feeding Rate X ₂ (kg/s)	Rotational Speed X ₃ (r/min)	Impurity Rate Y ₁ (%)	glume cluster rate Y ₂ (%)	Total Loss Rate Y ₃ (%)
1	29	2.5	900	29.24	25.55	0.83
2	29	2.5	700	21.36	31.40	1.80
3	29	1.5	900	27.40	26.44	0.71
4	29	1.5	700	22.37	28.04	1.32
5	21	2.5	900	36.29	13.30	1.13
6	21	2.5	700	31.65	22.25	0.54
7	21	1.5	900	32.87	20.02	0.49
8	21	1.5	700	30.53	16.40	0.82
9	31.728	2	800	23.87	30.79	1.63
10	18.272	2	800	35.94	18.81	0.76
11	25	2.841	800	38.40	19.56	0.70
12	25	1.159	800	25.28	14.89	0.26
13	25	2	968.2	31.01	19.99	0.55
14	25	2	631.8	21.63	26.23	0.67

Experime nt Number	Moisture Content X ₁ (%)	Feeding Rate X ₂ (kg/s)	Rotational Speed X ₃ (r/min)	Impurity Rate Y ₁ (%)	glume cluster rate Y ₂ (%)	Total Loss Rate Y ₃ (%)
15	25	2	800	31.68	18.49	0.46
16	25	2	800	35.34	15.77	0.75
17	25	2	800	37.93	18.76	0.49
18	25	2	800	26.85	24.21	0.77
19	25	2	800	30.57	23.92	0.71
20	25	2	800	30.43	23.41	0.74
21	25	2	800	27.91	18.87	0.93
22	25	2	800	23.19	25.93	0.78
23	25	2	800	33.63	23.04	0.71

To further elucidate the interactive effects of millet moisture content, feeding rate and rotational speed on the threshing and separating performance of the combined single longitudinal axial flow threshing and separation device, a multi-factor experiment was carried out using the orthogonal rotatable combination design method. The test results are presented in Table 4.

Regression analysis of the experimental data was performed using Excel software, and the regression equations for the impurity rate (Y_1) , glume cluster rate (Y_2) , and total loss rate (Y_3) with respect to the coded experimental influencing factors were established:

$$Y_1 = 30.851 - 3.754X_1 + 2.008X_2 + 2.611X_3 - 0.464X_1X_2 + 0.742X_1X_3 + 0.645X_2X_3 - 0.393X_1^2 + 0.294X_2^2 - 1.671X_3^2$$
 (2)

$$Y_2 = 21.376 + 4.365X_1 + 0.692X_2 - 1.703X_3 + 0.416X_1X_2 - 0.265X_1X_3 - 2.104X_2X_3 + 1.452X_1^2 - 1.245X_2^2 + 0.850X_3^2$$
 (3)

$$Y_3 = 0.702 + 0.230X_1 + 0.124X_2 - 0.111X_3 + 0.03X_1X_2 - 0.23X_1X_3 + 0.07X_2X_3 + 0.213X_1^2 - 0.042X_2^2 + 0.004X_3^2$$

$$\tag{4}$$

An error analysis was performed on Equations 2-4, and all regression equations met the criteria specified in Equation 5. This demonstrates that the regression model is statistically significant, and the models for each performance indicator are valid and meaningful.

$$F_{regression} > F_{0.05}(9,13) = 2.71$$
 (5)

Since the equation 6 is simultaneously satisfied, the lack of fit is not significant, indicating that the regression equation fits well.

$$F_{incompatibility} < F_{0.01}(5.8) = 6.63$$
 (6)

By substituting the coding formulas of the factor level coding table back into the above regression equation, the regression equation of the test index about the test factor value can be obtained. After eliminating the insignificant terms, the regression equations of each test indicator are as shown in Equation 7-9.

$$Y_1 = 25.3935 - 0.9385x_1 + 4.016x_2 + 0.0261x_3 \tag{7}$$

$$Y2=-2.8905-3.4463x_1+33.664x_2+0.0671x_3-0.0421x_2x_3+0.0908x_1^2$$
 (8)

$$Y3=-3.5232-0.1481x_1+0.248x_2+0.01327x_3-0.000575x_1x_3+0.0133x_1^2$$
 (9)

(2) Image analysis

The Origin and MATLAB software packages were utilized to generate single-factor and double-factor influence curves for the impurity rate, glume cluster rate and total loss rate. The underlying causes contributing to the observed curve patterns were subsequently analyzed.

Based on the single-factor and double-factor curves presented in Fig. 10, the following conclusions can be drawn. The impurity rate exhibits an inverse relationship with moisture content, increasing with higher

feeding rates and demonstrating a non-linear response to rotational speed, initially rising and subsequently declining.

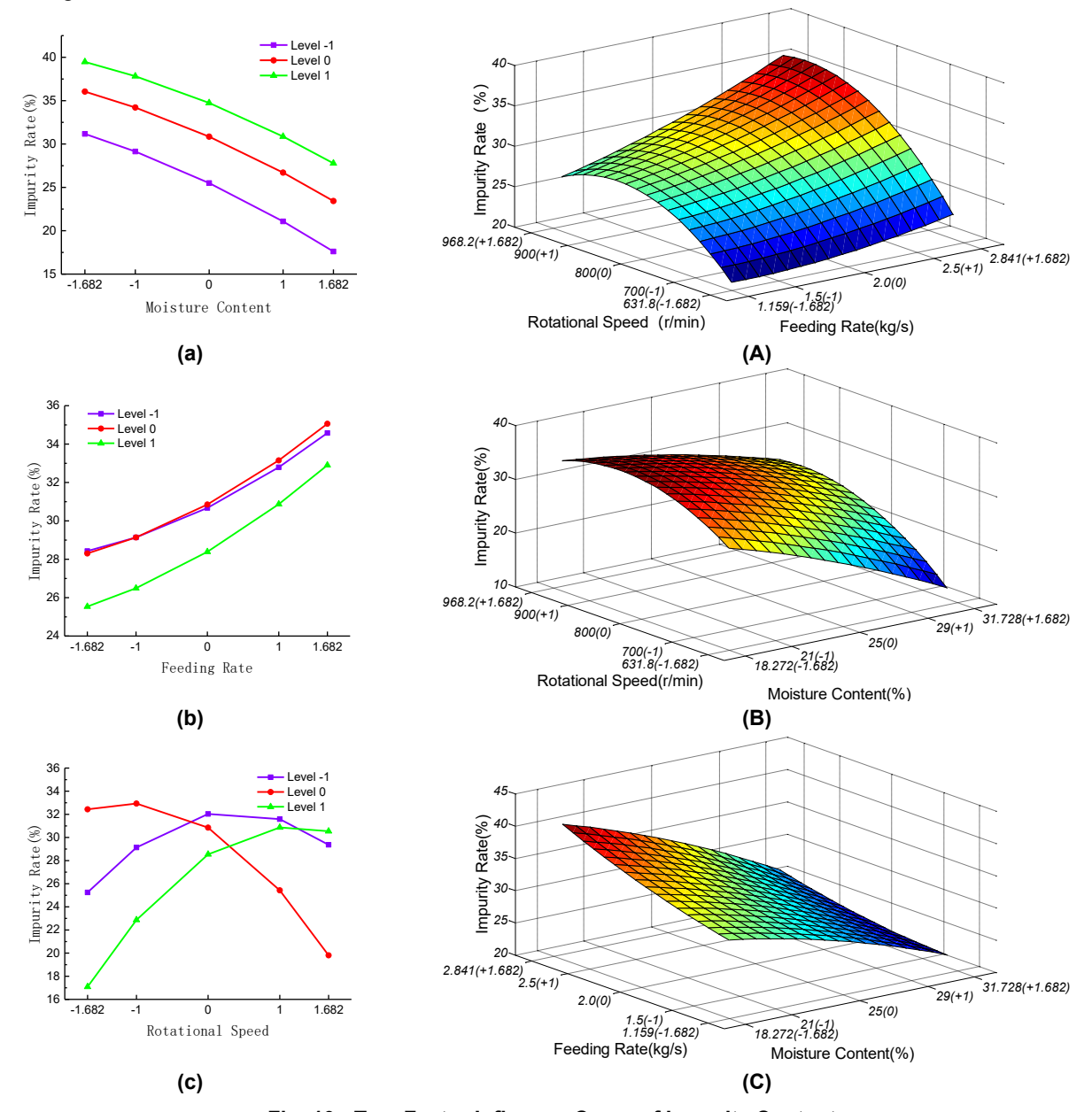


Fig. 10 - Two-Factor Influence Curve of Impurity Content

A decrease in moisture content increases the susceptibility of stems to breakage, thereby raising the impurity rate. Furthermore, under constant moisture content, higher feeding rate and rotational speed result in increased force exerted by the threshing device on materials within the axial flow threshing space. This increased force, coupled with a higher frequency of action, intensifies stem breakage and consequently raises the impurity rate. As the feeding rate increases, the density of the grain flow within the threshing space rises, leading to greater friction among the materials, threshing components, concave plate, and cover plate, which in turn enhances the likelihood of stem breakage and increases the impurity rate. An increase in rotational speed amplifies the impact and friction exerted by the threshing components on the materials, and the increased frequency of action further promotes stem breakage, thereby raising the impurity rate.

However, when the rotational speed continues to increase, the enhanced force facilitates the threshing of difficult-to-thresh grains, ultimately reducing the proportion of impurities in the threshed material.

Based on the contribution rate analysis, the order of influence of each experimental factor on the impurity rate is as follows: moisture content>rotational speed > feeding rate.

As illustrated in the single-factor and two-factor response curves in Fig. 11, the following conclusions can be drawn. The glume cluster rate generally increases with higher moisture content. The relationship

between feeding rate and glume cluster rate exhibits a non-linear trend, the glume cluster rate initially increases and then decreases as the feeding rate increases. Furthermore, when moisture content and feeding rate are at -1 and 0 levels, respectively, the glume cluster rate increases with rotational speed. Conversely, when both moisture content and feeding rate are at +1 level, the glume cluster rate decreases as rotational speed increases.

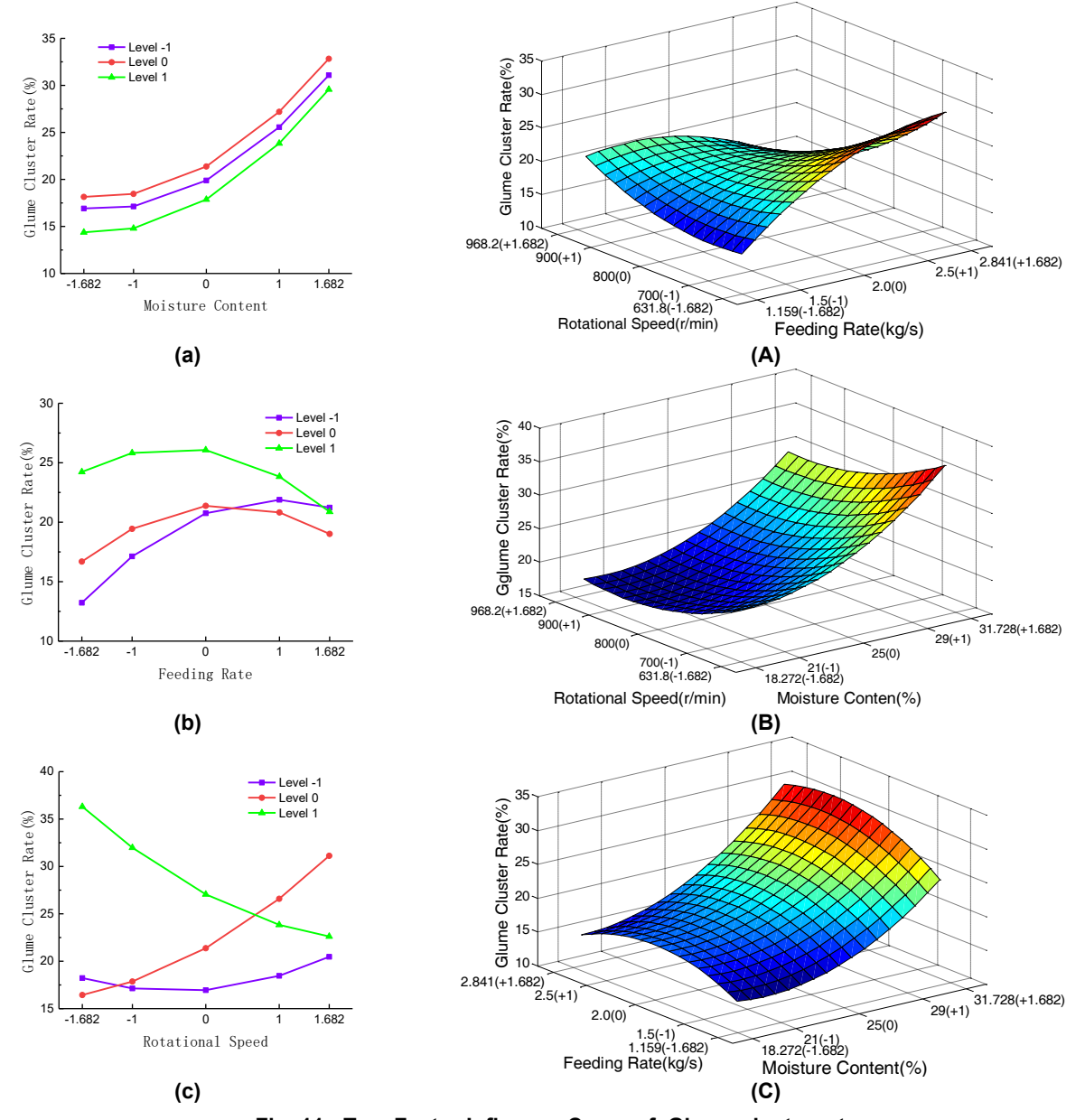


Fig. 11 - Two-Factor Influence Curve of Glume cluster rate

As the moisture content decreases, the bonding strength between the grain kernels and the glume clusters weakens, making the kernels more easily detached and resulting in a reduced proportion of remaining glume clusters. Under low feeding-rate conditions, the material layer within the axial-flow separation space becomes less dense, increasing the likelihood of grains being impacted and brushed by the threshing components. Consequently, the separated kernels can more easily pass through the loosely packed stem layer and fall through the concave openings, leading to a lower glume cluster rate. However, as the feeding rate increases, the material layer becomes denser and thicker, which reduces the effectiveness of impact and rubbing forces. This diminished separation intensity results in a higher proportion of glume clusters remaining unthreshed. When the feeding rate becomes sufficiently high, the increased friction between the material, the concave plate, and the cover plate promotes further detachment of kernels from the glume clusters, thereby reducing the glume cluster rate. As the rotational speed increases, both the frequency and intensity of impacts on the material within the separation space rise. Under conditions of low feeding rate and low moisture content, the sparse material flow and the reduced bonding strength between the glume clusters and the cob lead to a

gradual increase in glume cluster rate. In contrast, under high feeding-rate and high-moisture conditions, the increased material density within the separation space enhances inter-particle collisions and rubbing actions. These interactions facilitate more complete kernel detachment from the ears, resulting in a lower proportion of remaining glume clusters.

According to the contribution rate method, the order of the influence of each test factor on the glume cluster rate is: moisture content > rotational speed > feeding rate.

Based on the single-factor and two-factor curve graphs presented in Fig. 12, the following conclusions can be drawn. The total loss rate initially decreases and subsequently increases with rising moisture content. An increasing trend in the total loss rate is observed as the feeding rate increases. When moisture content and feeding rate are set at the -1 and 0 levels, respectively, the total loss rate increases with rotational speed. However, when both moisture content and rotational speed are at the +1 level, the total loss rate decreases as the feeding rate increases.

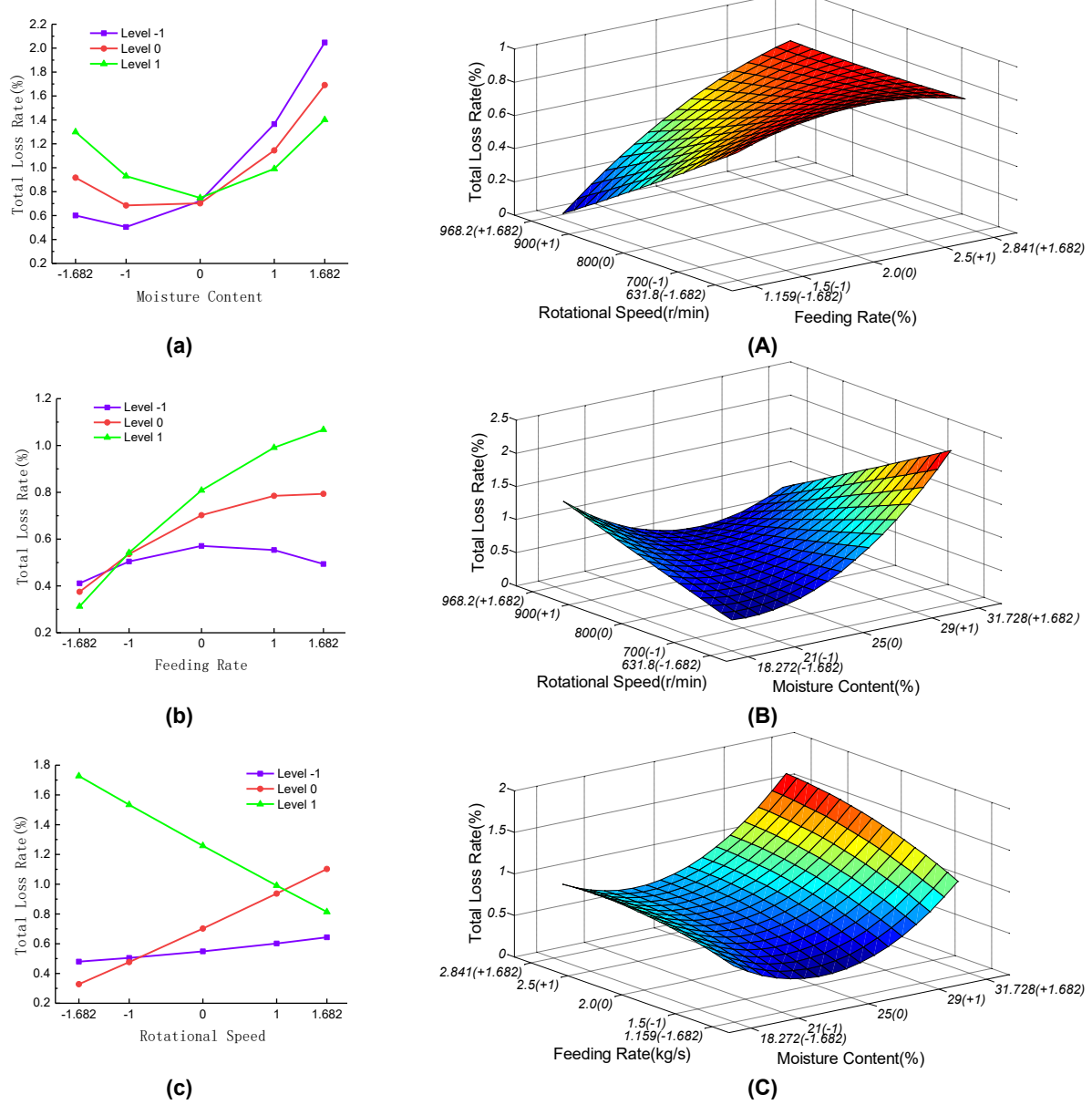


Fig. 12 - Two-Factor Influence Curve of Total Loss Rate

When the feeding amount remains constant, higher moisture content results in a sparser grain flow within the threshing space, thereby enhancing the effectiveness of the threshing components on the grains. As a result, the threshed grains can more easily pass through the sparse material layer, leading to a gradual decrease in the total loss rate. However, as the moisture content continues to increase, the bonding force between individual grains and the grain bundles, as well as between the grain bundles and the cob, also increases. This makes the occurrence of unthreshed grains more likely.

Additionally, the number of broken grain bundles within the axial-flow threshing space increases, and these broken bundles are much more difficult to separate through the material layer than individual grains.

Consequently, carryover loss increases, ultimately leading to a rise in the total loss rate. When the feeding volume increases, a larger amount of material accumulates within the axial-flow threshing space, resulting in insufficient interaction between the threshing components and the crop material. In addition, the threshed grains face greater difficulty passing through the thickened material layer, which further increases carryover losses.

Under the same feeding volume, higher moisture content and higher rotational speed both correspond to increased total loss rate. This is because elevated moisture content increases the proportion of broken grain bundles, while higher rotational speed intensifies material breakage. Both factors contribute to a higher total loss rate. When both moisture content and feeding rate are at the -1 level, an increase in rotational speed enhances the impact force and contact frequency between the material and threshing components, causing the grain flow in the separation space to become sparser.

As a result, the grains are more effectively threshed and separated into the receiving unit, and the total loss rate decreases with increasing rotational speed. When the feeding rate and moisture content rise to the 0 level, the quantity of material in the threshing space increases.

As the rotational speed increases, the stems become more susceptible to breakage, and some already-threshed grains encounter greater difficulty passing through the thickened and fragmented stem layer, thereby increasing the total loss rate. When the feeding rate and moisture content increase to the +1 level, the stems become less prone to breakage. Under these conditions, higher rotational speed increases the stirring frequency of the threshing components, enabling more separated grains to pass through the material layer and fall into the receiving unit, thus reducing the total loss rate.

Based on the contribution rate analysis, the order of influence of the test factors on the total loss rate is: moisture content > rotational speed > feeding rate.

4. Experimental Optimization

The Design-Expert software was employed to optimize the experimental parameters, resulting in the following optimal combination of factors: a moisture content of 24.82%, a feeding rate of 2.25 kg/s, and a rotational speed of 835 r/min. To validate the optimization outcomes, experiments were conducted three times under these conditions, and the average values were calculated. The final results showed an impurity rate of 31.90%, a glume cluster rate of 21.56%, and a total loss rate of 0.72%.

CONCLUSIONS

- (1) As moisture content increases, the impurity rate decreases, the glume cluster rate increases, and the total loss rate first decreases and then increases. With increasing feeding rate, both the impurity rate and the total loss rate show an overall upward trend, while the glume cluster rate initially increases and then decreases. As rotational speed increases, the impurity rate first rises and then falls. When both moisture content and feeding rate are at low levels, the glume cluster rate increases with increasing rotational speed. In contrast, when moisture content and feeding rate are at high levels, both the glume cluster rate and the total loss rate decrease as rotational speed increases.
 - (2) Based on the contribution rate analysis, the order of influence of the test factors is as follows:
 - For impurity rate: moisture content > rotational speed > feeding rate;
 - For glume cluster rate: moisture content > rotational speed > feeding rate;
 - For total loss rate: moisture content > feeding rate > rotational speed.
- (3) The optimal operating parameters for the single longitudinal axial flow threshing and separation device equipped with the rasp-bar and nail-tooth combined threshing element are: a moisture content of 24.82%, a feeding rate of 2.25 kg/s, and a rotational speed of 835 r/min. Under these conditions, the impurity rate is 31.21%, the glume cluster rate is 19.73%, and the total loss rate is 0.73%.

REFERENCES

- [1] Amir, H. M., & Gholam, R. C. (2015). Measuring Picking Force of Sunflower Seeds and Prediction of Reasonable Range of Air-jet Parameters to Remove Sunflower Seeds from the Head [J]. *Agriculture Engineering International: CIGR Journal.* 17(3):415-429.
- [2] Amir, H.M., & Gholam, R.C. (2016). Effect of Air-jet Impingement Parameters on the Removing of Sunflower Seeds from the Heads in Static Conditions [J]. *Agriculture Engineering International: CIGR Journal*. 18(2).

- [3] Atis, I., Konuskan, O., Duru, M., Gozubenii, H. & Yilmaz, S. (2012). Effect of Harvesting Time on Yield, Composition and Forage Quality of some Forage Sorghum Cultivars [J]. *Int. J. Agric. Biol.* (14): 879-886.
- [4] Dainius, S., Aurelija, K., Edvinas, P., & Rolandas, D. (2023). Shape Optimization of Concave Crossbars to Increase Threshing Performance of Moist Corn Ears [J]. *Agriculture*. 13(5).
- [5] Fozilov, G., Akhmedov, A., Yuldashev, Sh., Akilova, U., Juraev, K. (2025). Theoretical study of the threshing process of corn cob under the influence of the rasp bars [J]. *IOP Conference Series: Earth and Environmental Science*. 1420(1): 012031.
- [6] Gorji, A., Rajabipour, A., & Tavakoli, H. (2010). Fracture Resistance of Wheat Grain as a Function of Moisture Content, Loading Rate and Grain Orientation [J]. Australian Journal of Crop Science. 4(6): 448-452.
- [7] Hou, S., & Chen, H. (2012). Parameters Optimization of Vertical Axial Flow Thresher for Soybean Breeding [J]. *Transactions of the Chinese Society of Agricultural Engineering*. 28(5): 19-25.
- [8] Kang, D., Wu, C. Y., Liang, S., & Tang, Q. (2017). Design and Test of the Threshing Device of Millet Combine Harvester (谷子联合收获机脱粒装置设计与试验) [J]. *Journal of China Agricultural University*. 22(02): 135-143.
- [9] Luo, H.G., Shi, Q.X., Wang, G.S., Geng, L. X., & Xu, Z. (2016). Experiment of Millet Head-feed Threshing Unit (谷子半喂入脱粒装置试验) [J]. *Journal of Henan University of Science and Technology (Natural Science*). 37(5): 56-61.
- [10] Martynas, M., Niels, P., Greta, M., Mantas, P., & Dainius, S. (2025). Crop Flow Control in a Longitudinal Axial Threshing Unit Using Fully Adjustable Guide Vanes: A Field Study in Winter Wheat Harvesting [J]. *Applied Sciences*. 15(12): 6864.
- [11] Maundc, F.A. (2011). Performance Evaluation of Manual Cowpea Thresher [J]. *African Journal of Agricultural Research*. 6(30): 6412-6415.
- [12] Mingrui, L., Yanchun, Y., Yongkang, Z., Xibin, L., Dong, Y., & Duanyang, G. (2025). Design and Experiment of a Double Longitudinal Axial-flow Corn threshing Device for Large Feeding Capacity [J]. *INMATEH Agricultural Engineering*. 75(1): 75-45.
- [13] Nnam, I.O., Uzoechi, S.G., Otuu, O. I., & Ibiam, N.O. (2025). Development of a Mobile Motorized Rice Threshing Machine for Small and Medium Scale Rice Farmers [J]. Asian Journal of Advanced Research and Reports. 19(7): 194-203.
- [14] Panpan, L., Zheng, L., Jin, W., Lulu, L., Anqi, J., Han, Y., & Chengqian, J. (2025). Effects of Moisture Content on Mechanical Crushing Performance of Soybean Seeds and Its Application in Mechanized Harvesting [J]. *INMATEH Agricultural Engineering*. 75(1): pp.231-242. DOI: https://doi.org/10.35633/inmateh-75-20
- [15] Solomon, T. H., Mersha, A., Mulugeta, A. D., & Addisu, N. A. (2024). Effects of machine-crop parameters on mechanical grain damage in rice threshing [J]. *Cogent Food & Agriculture*. 10(1).
- [16] Tiwari, R. K., & Chauhan, S. K. (2018). Investigations on effect of cylinder configuration of rectangular spiked tooth thresher on threshing performance of wheat crop [J]. *Indian Journal of Agricultural Research*. 52(5): 560-565.
- [17] Ukatu, A.C. (2006). A Modified Threshing Unit for Soya Beans [J]. *Biosystems Engineering*. 95(3):371-377.
- [18] Wang, S., Shi, Q. X., Geng, L. X., & Luo, H. G. (2016). Development of Test-bed of Semi-feeding Millet Threshing Mechanism (谷子半喂入脱粒装置试验台设计) [J]. *Journal of Chinese Agricultural Mechanization*. 37(12): 27-30.
- [19] Wuttiphol, C., & Somchai, C.U. (2018). Factors of Operation Affecting Performance of a Short Axial-flow Soybean Threshing Unit. *Engineering Journal*. 22(4).
- [20] Yanqing, Z., Qingliang, C., & Hongbo L. (2018). Effects of Stem Region, Moisture Content and Blade Oblique Angle on Mechanical Cutting of Millet Stem [J]. *INMATEH-Agricultural Engineering*. 2(55): 105-112.
- [21] Zhang, Y. Q., Cui, Q. L., & Xin L. (2019). Variations and Correlations of Shearing Force and Feed Nutritional Characteristics of Millet Straw [J]. *Transactions of the Chinese Society of Agricultural Engineering (Transactions of the CSAE*). 35(5): 41-50.